Cleaner Materials 1 (2021) 100017

Contents lists available at ScienceDirect

Cleaner Materials

journal homepage: www.elsevier.com/locate/clema

Engineering properties, phase evolution and microstructure of the iron-rich aluminosilicates-cement based composites: Cleaner production of energy efficient and sustainable materials

Van Essa L.K. Samen [a,b,*], Rodrigue Cyriaque Kaze [c], Juvenal Giogetti Deutou Nemaleu [a], H.K. Tchakoute [c], P. Meukam [b], E. Kamseu [a,d,*], C. Leonelli [d]

[a] Local Materials Promotion Authority (MIPROMALO), P.O. Box 2396, Yaoundé, Cameroon
[b] Laboratoire Eau, Energie, environnement, Ecole Nationale Polytechnique de Yaoundé, P.O. Box 8390, Yaoundé, Cameroon
[c] Laboratory of Applied Inorganic Chemistry, Faculty of Science, University of Yaoundé I, P.O. Box 812, Yaoundé, Cameroon
[d] Department of Engineering Enzo Ferrari, University of Modena and Reggio Emilia, Via Vignolese 905/A, 41 125 Modena, Italy

ARTICLE INFO

Keywords:
Laterites
Particle size distribution
Microstructure
Pore size distribution
Mechanical properties

ABSTRACT

This paper investigates the direct transformation of laterites (natural iron-rich aluminosilicates) to cementitious composites with principal mineral phases being Gismondine and Stratlingite. The effects of particles size distribution and cement content (2 to 8 wt%) on the mechanical properties and microstructure of laterite-cement composites are assessed. Four grades of granulometry with various percentages of fine and coarse particles were considered. The Environment Scanning Electron Microscopy (ESEM), Mercury Intrusion Porosimetry (MIP), Fourier Transformed Infrared Spectroscopy (FT-IR) and X-ray Powder Diffractometry (XRD) were performed after 1, 90 and 365 days, to assess the phase's evolution, mechanical performance and the microstructure of the laterite-cement composites. It is found that fines particles, essentially pozzolanic and amorphous, are responsible for the bonding strength while coarse particles improve the compressive strength. Dense and compact microstructure, water absorption under 18% and flexural strength above 6 MPa (compressive strength > 30 MPa) could be achieved as from 4 wt% of cement making the laterite-cement composite appropriate as building and construction materials. The choice of a highly corroded class of laterite and the selection of the particle size distribution allows the production of optimum composite that is presented as energy-efficient and sustainable. Thus, corroded or indurated laterites are considered as "green metakaolins" which do not require any energy for their transformation unlike clayey materials.

Introduction

Cleaner production emphasizes both energy and resource-efficiency improvements, and many of the requirements relating to the reduction of greenhouse gas emissions, waste minimization, and environmental protection. Calcinated clays are generally promoted as eco-friendly materials with applications as a supplement for Portland Cement and an agent for the improvement of the durability of concretes (Tironi et al., 2013; Fernandez et al., 2011; Zhang et al., 2018; Forster et al., 2020; Kaze et al., 2018). In the tropical region of the world, kaolinite in contact with iron minerals develops a particular class of raw materials called laterites (Kasthurba et al., 2008; Kasthurba et al., 2007; Jaritngam et al., 2014). This natural transformation, without energy input, makes laterites appears as a "green raw material" ready to be converted to cementitious phases in the presence of hydrated cement. The conversion, with the save of the energy need for the thermal calcination of laterite is environmentally friendly with low CO_2 emission and can be called energy efficiency process in relation with the cleaner production.

Laterites are iron-rich aluminosilicates generally presenting SiO_2/Al_2O_3 and SiO_2/R_2O_3 molar ratios less than 1.33 (R = Fe, Ti, Al). The presence of a significant fraction of iron is one of the most important factors that influence the engineering properties of laterites. Well laterized crusts can present up to 34–40 wt% of iron oxides and hydroxides. During the phenomenon of laterization, the iron cations penetrate into the clay (kaolinite) structure and substitute many of the Al^{3+} ions and even Si^{4+}. This substitution results to the structural deformation of the kaolinite with a certain level of disorder that allows

* Corresponding authors at: Local Materials Promotion Authority (MIPROMALO), P.O. Box 2396, Yaoundé, Cameroon.
E-mail addresses: liliane.sk16@gmail.com (V.E.L.K. Samen), giogetti@live.fr (J.G. Deutou Nemaleu), kamseuelie2001@yahoo.fr (E. Kamseu).

https://doi.org/10.1016/j.clema.2021.100017
Received 8 July 2021; Revised 23 August 2021; Accepted 1 September 2021

the formation of a significant semi-crystalline and metastable fraction (Kaze et al., 2018; Kaze et al., 2017). The iron-rich aluminosilicates become then favourable to the development of pozzolanic reactions in the presence of cement (Jaritngam et al., 2014; Jaritngam et al., 2013; Changling, 1969). In those laterites, amorphous and disordered $Al_2O_3.2SiO_2$ (AS_2), $Al_2O_3.4SiO_2$ (AS_4), Fe_2O_3 (F) and FeO(OH) (FH) can be found. In the presence of water, C_2S and C_3S are transformed to CSH and CH as indicated with the equations (1) and (2).

$$2C_3S + 6H \rightarrow C_3S_2H_3 + 3CH \quad (1)$$

$$C_2S + 4H \rightarrow C_3S_2H_3 + CH \quad (2)$$

AS_2 and AS_4 react with $Ca(OH)_2$(CH) to form some hydrates of alumina bearing phases (Tironi et al., 2013; Tironi et al., 2015) as can be indicated with the equations (3) and (4);

$$4CH + AS_2 + (FH) \rightarrow C_4AS_2FH_5 \quad (3)$$

$$6CH + AS_4 + (FH) \rightarrow C_6AS_4FH_7 \quad (4)$$

The reactions (3) and (4) are pozzolanic and are essentially associated to the level of disorder into the kaolinic structure of laterites. Similar pozzolanic reactions are extensively described into the literature when using calcinated kaolin (metakaolin) to stabilize the residual CH, product of the cement hydration or when developing alternatives binders made from metakaolin and lime (Fernandez et al., 2011; Tironi et al., 2015).

Goethite (FH) can be transformed in hematite phases according to equation (5).

$$2FeO(OH) \rightarrow Fe_2O_3 + H_2O \quad (5)$$

In the well laterized materials, the above physico-chemical reactions would take place in alkaline conditions leading to a complex microstructure in which many cementitious minerals densify the system and provide enough strength. The laterite directly reacts with cement without any thermal transformation (calcination). However, although the largely availability of the materials in the tropical area, many works undertaken in the field of laterites based composites adding cement suffer from poor mechanical properties, low densification and high-water absorption making those materials appear as second class or non-appropriate for engineering applications (Kasthurba et al., 2008; Jaritngam et al., 2014; Obonyo et al., 2014; Lasisi et al., 1990; Omotoso et al., 2012). Kasthurba et al. (2007) studied the influence of a quarry depth on laterite engineering properties. They found a maximum compressive strength of about 2.2 MPa with a water absorption under 15%. They concluded that, the engineering properties are better when laterite is extracted from the surface of the quarry because of a high iron content. However, explanations on the action of iron within the material have not really been highlighted in order to justify this trend, although the compressive strength remain low compared to those of conventional materials. Billong et al. (2009) on the other hand, studied the properties of a stabilized earth blocks with burnt clay–lime at 20 and 30%. They succeed to obtain a maximum compressive strength of 10 MPa and conclude that the increase of the percentage of binder is responsible for the increase of the final product's compressive strength. However, even if the binder plays an important role in the improvement of the properties of final products, the nature of the laterite together with the particle size have also a determining role. In fact, the chemical composition of laterites respects the requirement of ASTM C618 concerning the evaluation of natural pozzolans (Kaze et al., 2017; Pourkhorshidi et al., 2010); with $SiO_2 + Al_2O_3 + Fe_2O_3$(FeO) that is generally above 70 wt%. The level of laterization is proportional to the effectiveness of the formation of binder from pozzolanic reactions. In the presence of cement, the action of iron participating to the binder formation depends on the crystalline nature of the parent minerals. Quartz and iron (hydroxide) have reactive surfaces often associated with one to another in soils and sediments. Studying the quartz-silica coating, with iron hydroxide (FeO(OH), goethite) and iron oxide (Fe_2O_3, hematite), Rusch et al. 2010 showed that the surface of hydroxyls of quartz can be involved into the coating process, providing a strong bonding between the coating iron oxides and the silica surface. The presence of soluble silica has an impact on the reactivity of goethite crystallites which have small size and higher surface area. Silicates can be covalently bonded to goethite surface by replacement of OH group. In the laterite, iron can be found as ferrihydrites, goethite, hematite and lepidocrocite: the amorphous form of goethite being the mineral with the major reactive potential. Considering the presence of quartz, sand and cement, the following reactions can take place when the pH of the system is above 9.

$$SiO_2 + 2OH^- \rightarrow H_2SiO_4^{2-} \quad (6)$$

$$Fe(OH)_2 + H_4SiO_4 \rightarrow Fe^{2+} + H_2SiO_4^{2-} + 2H_2O \rightarrow FeH_2SiO_4 \cdot 2H_2O \quad (7)$$

Fresh ground fines particles of high grade of laterized materials are expected to develop good physico-chemical bonds developing cementitious phases capable of densifying and strengthening the laterite-cement composites in the same manner as any other pozzolanic materials. The resulting composites are products with high potential of sustainability with respect to the calcined clay added cement. Kaolin is generally calcined at the temperature range between 700 and 850 °C consuming 600–700 Kcal/Kg. This quantity of energy is associated with 200–300 Kg of CO_2 emitted per ton of calcined kaolin in view to obtain amorphous metakaolin (Fernandez et al., 2011; Maddalena et al., 2018; Alujas et al., 2015; Yanguatin et al., 2017). The use of laterite in this project allows to save the energy of calcination, the emissions of CO_2 and related greenhouses gazes making the aim products viewed as energy efficient and sustainable materials.

The objective of this work is to highlight the effect of the particles size of raw laterite within the matrix and to demonstrate the impact of iron ions contained in laterite on the engineering properties. This is achieved through the study of the phase evolution, the densification process, the microstructure and the porosity of laterite-based composites. The mechanical properties (compressive and flexural strength) and linear shrinkage are used for the evaluation of the cementitious phases formed; those phases are assessed using FT-IR spectroscopy and XRD. Water absorption and Mercury Intrusion Porosimetry are used to compare the quality of products with existing structural materials for building and construction.

Materials and methods

Materials and samples preparation

Laterite was collected at Obili neighbourhood in Yaoundé (Centre region in Cameroon). The laterite was dried (sun drying), crushed and then sieved. Two fractions were considered after sieving: the fine particles series ($\phi \leq 1$ mm; including nano and micro particles) and coarse particles (1 mm $\leq \phi \leq$ 4 mm). The cement used was a Portland cement (CEM II 42.5) from Dangote cement factory, Douala Cameroon. This cement contains clinker (70–79 %), pozzolan (21–25 %) and gypsum (≤5 %). Its fineness is between 3900 and 4000 cm^2/g. The mineral phases of laterite are quartz, kaolinite, hematite, goethite, anatase, and lepidocrocite (Kaze et al., 2017) while CEM II 42.5 presented: Alite, Belite, quartz, calcite, pyroxene and plagioclase. Pyroxene and plagioclase are residual crystalline phases of volcanic ash used as additives (Jean Noël et al., 2020; Djobo et al., 2017; Leonelli et al., 2007; Kamseu et al., 2016).

The bulk chemical composition of laterites and cement are summarized in Table 1. Four powders of different fines/coarse ratio (100/0, 75/25, 50/50 and 25/75) were prepared. To each powder 2, 4, 6

Table 1
Chemical compositions of raw materials.

Oxides (wt. %)	Laterite	Cement
Fe_2O_3	37,5	4,65
SiO_2	25,1	19.3
Al_2O_3	23	5,5
TiO_2	0,9	/
V_2O_5	0,15	/
P_2O_5	0,14	/
Cr_2O_3	0,23	/
CaO	0.29	65
MgO	0.07	0,98
CaO free	/	1,8
K_2O	1.8	0.9
SO_3	Not detectable	2.01
Na_2O	0.2	0.2
LOI	10,6	0.45

and 8 wt% of cement were added. The amount of water added to each formulation before pressing varied from 6 to 11 vol% according to the fines content: the powder 25/75 with the higher amount of coarse laterite received 6 vol% of water while 100/0, 75/25 and 50/50 received respectively 11, 10 and 7 vol%. The mentioned water content corresponds to the amount of water needed to achieve self-compaction of each mix powder. After the addition of water, the slurry was mixed for 5 min using the Hobart mixer (model N50_G). The mixture was then poured in the mold (205 mm × 95 mm × 35 mm) and pressed up to 140 bars. The apparatus used to realize specimens was Nannetti Brand press machine with a hydraulic system. The total mass of laterite, cement and water was 1400 g for each specimen. Finally, specimens were identified as presented in Table 2.

The blocks were wrapped into plastic for the first 28 days to avoid water evaporation during the curing process and curing for a period of 90 and 365 days continued at room temperature.

Characterization of LAT-CEM composites

Mechanical and physico-chemical properties

Three-point flexural and compressive strength testing of the samples were performed using an ELE International machine with a displacement rate of 3 mm/min. The results shown are an average of a minimum of three replicate specimens tested. The mechanical test was performed following as much as possible the American Standard regarding the three-point flexural strength testing, ASTM C78/C78M – 02 (ASTM C78/C78M-02, 2002) and the compressive strength testing, ASTM C 39/C 39M – 05 (ASTM C39/C39M-05, 2005).

Considering the dimensions of the specimens, 205 mm × 95 mm × 35 mm and the spam 150 mm, the maximum flexural strength was calculated using the equation (8):

$$\sigma = \frac{3 \times F \times D}{2 \times l \times h^2} \tag{8}$$

where σ is the maximum centre tensile stress (MPa), F maximum load at fracture (N), D the distance between the supports (mm), l the width and h the thickness of the specimen (mm).

For the maximum compressive strength, the formula is given by the equation (9):

$$R_c = \frac{F}{h \times l} \tag{9}$$

where Rc is the maximum compressive stress (MPa), F the load of crushing (N), l the width and h the thickness of the specimen (mm).

The water absorption (WA) analysis was carried out by immersing the specimen in water at ambient temperature for 24 h and comparing the humid weight (m_h) to the initial dry weight (m_s) according to the equation (10). The water absorption test was carried out follow as possible the ASTM standard C373-88 (C. ASTM, 2008).

$$W_a(\%) = \frac{m_h - m_s}{m_s} \times 100 \tag{10}$$

where m_h is the wet mass and m_s is the dry mass.

The bulk density and apparent porosity were determined by the Archimedes method according to the ASTM standard C373-88 (C. ASTM, 2008) using the analytical balance with ±0.0001 g sensitivity.

For all the different analysis, three representative test specimens were used to evaluate the mean values and standard deviation.

Phases evolution, mercury intrusion porosimetry and microstructure

Fourier Transformed Infrared Spectroscopy, FT-IR using Avatar 330 FT-IR, Thermo Nicolet was performed on selected samples. The analysis was done on the pieces collected from the mechanical testing allowing to have access to the surface and the bulk. A minimum of 32 scans between 4000 and 400 cm^{-1} were averaged for each spectrum at the intervals of 1 cm^{-1}. The pieces were ground finely under 80 μm before analysis.

Mineralogical analysis of the LAT-CEM composites was carried out with an X-ray powder diffractometer, XRD, (PW3710, Phillips) Cu Kα, Ni-filtered radiation (the wavelength was 1.54184 Å). The radiation was generated at 40 mA and 40 kV. The analysis was performed on fine grains of ground samples. Specimens were step-scanned as random powder from 5° to 70°, 2θ range, and integrated at the rate of 2 s per step. Acquisition and processing of data was carried out using the Philips High Score software package by comparing the pdf of mineral phases obtained with the pdf ICCD data.

Pieces collected from the mechanical tests were used to prepare specimens of ~1 cm^3 of volume for the Mercury Intrusion Porosimeter (MIP) (Auto pore IV 9500, 33000) analysis using psia (228 MPa). Mercury Intrusion Porosimetry (MIP) covering the pore diameter range from 0,01 to 360 μm having two low-pressure ports and one high-pressure chamber.

For the Environmental Scanning Electron Microscope (ESEM), pieces from mechanical tests were collected and dry cut parallel to fracture surface with the diamond saw to observe the fractures surfaces. The specimens chosen had various interfacial aggregate/matrix zones. A backscattered electron (SSD) detector was used to acquire images. The principle of the SSD is that the intensity at which electrons are backscattered depends on the local atomic number and topography of the specimen. The pores, as absence of solid, do not scatter electrons and appear uniformly black.

BET surface area of cement and laterite

The specific surface area of iron rich aluminosilicates powder was determined according to the Brunauer-Emmet-Teller (BET) method

Table 2
Mix-design of the laterite-cement composites.

X/Y	2 wt% of cement	4 wt% of cement	6 wt% of cement	8 wt% of cement	Wt % water
100/0	LAT-CEM 100/0-2	LAT-CEM 100/0-4	LAT-CEM 100/0-6	LAT-CEM 100/0-8	11
75/25	LAT-CEM 75/25-2	LAT-CEM 75/25-4	LAT-CEM 75/25-6	LAT-CEM 75/25-8	10
50/50	LAT-CEM 50/50-2	LAT-CEM 50/50-4	LAT-CEM 50/50-6	LAT-CEM 50/50-8	7
25/75	LAT-CEM 25/75-2	LAT-CEM 25/75-4	LAT-CEM 25/75-6	LAT-CEM 25/75-8	6

based on nitrogen absorption. The analysis was done using a micrometrics GEMINI 2360 instruments.

Results

Phases evolution

The FT-IR spectra of laterite-cement composites with 8 wt% at 1 day and 90 days are depicted in Fig. 1 (a and b). On the spectrum of laterite-cement composite at 1 day, absorption bands situated at 3610 and 3695 cm^{-1} are characteristics of OH bonds that may be from kaolinite and goethite (Kaze et al., 2017). The absorption bands disappeared with the reaction of cement and laterite (Fig. 1a), implying that the kaolinite and goethite have been effectively transformed to new binding phases (C-A-S-H, Equations (3) and (4)). The bands at 1639 and 3403 cm^{-1} on spectra of laterite-cement composites cured at 1 day, are attributed to the O-H stretching and H-O-H bending vibration modes (Kapeluszna et al., 2017). Those bands significantly lose intensities when the reaction with cement is effective. This is due to the departure of water molecules out of matrix after the dissolution and polycondensation reactions; and development of a compact structure. The same behaviour was proven by Latifi and co-workers (Latifi et al., 2014), on laterite soil treated with sodium silicate-based liquid stabilizer. In fact, the cement used is predominantly C-S-H phases after hydration while sodium silicates are N-S-H phases: two well-known alkaline based binders. They concluded that the reduction of peaks intensity of H-O-H with curing time is due to the weathering action of the stabilizer on the clay minerals. The weathering action is as fast as the clay minerals into the laterite are corroded by iron making the structure weaker, vulnerable to alkaline attack. The absorption bands between 1409 and 1442 cm^{-1} are ascribed to stretching of C-O bonds, which are found in all FT-IR spectra of specimens cured at 90 days due to the formation of sodium carbonate from the reaction of alkali metal with CO_2. However, the peaks intensities of C-O bonds are very low suggesting a very good stability of the C-A-S-H phases formed and the quasi absence or very low content of residual alkali-based compounds into the system. The principal peak showing the aluminosilicate nature of laterites (Kapeluszna et al., 2017; Latifi et al., 2014; Yu et al., 2004) shifted to higher values of wavelength: 1027 cm^{-1} (LAT-CEM 50/50) and 1031 cm^{-1} (LAT-CEM 100/0, LAT-CEM 75/25 and LAT-CEM 75/25) confirming the incorporation of Si into the system. In fact, the LAT-CEM 100/0 composite with just 1 day of curing present peaks of C-S-H around 1080–1100 cm^{-1} after those of 3400 and 1639 cm^{-1} (Millogo et al., 2008; Millogo, 2008) and the principal peak of aluminosilicate at 1024 cm^{-1}. The peaks at 912–914 cm^{-1} in the LAT-CEM composites with complete curing appears at 908 cm^{-1} in the specimen having only 1 day of curing. In fact, at 1 day, the reactions between C-S-H and laterite are still to be completed. The peak essentially indicates the level of reactivity means the formation of C-A-S-H systems. Its intensity increases significantly in the specimens with complete curing showing the effective development of the cementitious binder. Between 900 and 400 cm^{-1}, there are series of small peaks with increase intensities when the reactions LAT-CEM are completed. Those peaks also evidence the formation of C-A-S-H as it can be confirmed by the literature (Horgnies et al., 2013; Kapeluszna et al., 2017; Latifi et al., 2014; Yu et al., 2004; Millogo et al., 2008).

The X-ray patterns of laterite-cement composites aged of 1, 90 and 365 days are depicted in Fig. 2 (a, b and c). The main mineral phases identified at 1 day are Ettringite (E) ($Ca_6Al_2(SO_4)_3(OH)12{\cdot}26H_2O$), Kaolinite (K) ($Al_2Si_2O_5(OH)_4$), Portlandite (P) ($Ca(OH)_2$), Quartz (Q) ($SiO_2$), Hematite (He) ($Fe_2O_3$), Goethite (Go) (FeO(OH)) and Calcium Silicate Hydrated (C-S-H). Those phases are embedded in an amorphous matrix of laterite which at that stage has reacted partially. While kaolinite, goethite, hematite and quartz are parent mineral of laterite, ettringite, portlandite and C-S-H are essentially the products of hydration and partial reactivity of laterite. Phases like ettringite, goethite and C-S-H present in the 1 day specimen are transformed after 90 days of curing to new stable phases like Gismondine (Gi) ($CaAl_2Si_2O_8{\cdot}4(H_20)$), Stratlingite (S) ($Ca_2Al_2(SiO_2)(OH)_{10}{\cdot}2.5H_2O$) and C-A-S-F-H. The overall level of crystallinity of the matrix is enhanced at 90 days of curing. Situation that is confirmed and improved at 365 days.

Portlandite, which is the result of self-hydration of cement, is generally more visible up to the seven first days of curing (Jaritngam et al., 2014; Jaritngam et al., 2013; Jaritngam et al., 2012; Lucia, 2011; Awoyera et al., 2018; Tajuelo Rodriguez, 2015) as observed in the results obtained with XRD. Its presence at 1 day curing and total disappearance at 90 and 365 days indicates that the reaction of the hydration of cement in the presence of laterite took place as usual: hydration with formation of C-S-H and portlandite: equations (1) and (2).

The sequences of the reactions continue with portlandite that react with laterite as described in the equations (3) and (4).

Those pozzolanic reactions that follow the bonding of C-S-H with laterites (Al, Si, Fe) are responsible for the formation of C-A-S-H and C-A-S-F-H which in this case are gismondine ($CaAl_2Si_2O_8{\cdot}4(H_20)$) and stratlingite (S) ($Ca_2Al_2(SiO_2)(OH)_{10}{\cdot}2.5H_2O$).

LAT-CEM 100/0, LAT-CEM 75/25, LAT-CEM 50/50 and LAT-CEM 25/75 presented similar mineral phases at 90 days with 8 wt% of cement content (gismondine, stratlingite, C-A-S-F-H and hematite) with the only difference linked to peaks intensity (Fig. 3). The presence of the original phase as goethite that can be easily dissolved by

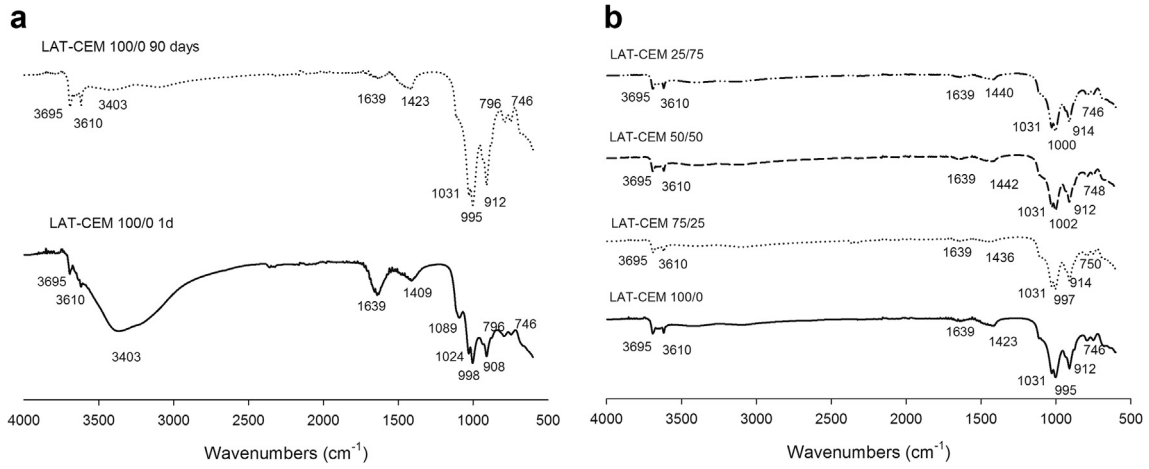

Fig. 1. FT-IR spectra (a) of LAT-CEM 100/0 at 1 day and at 90 days respectively and (b) different formulations at 90 days.

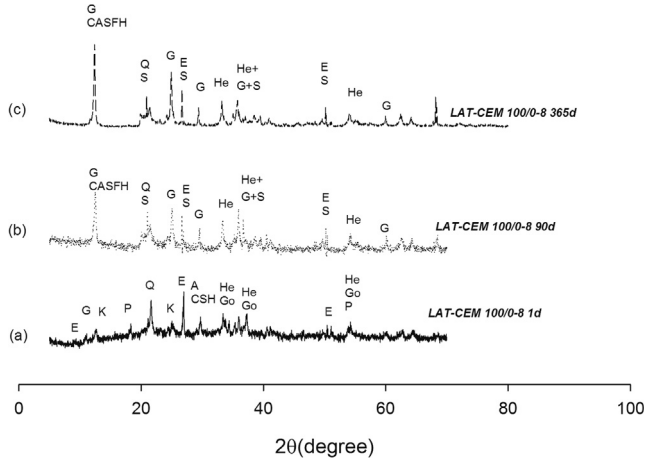

Fig. 2. XRD patterns of LAT-CEM 100/0 with 8 wt% of cement content at: (a) 1 day, (b) 90 days and (c) 365 days.

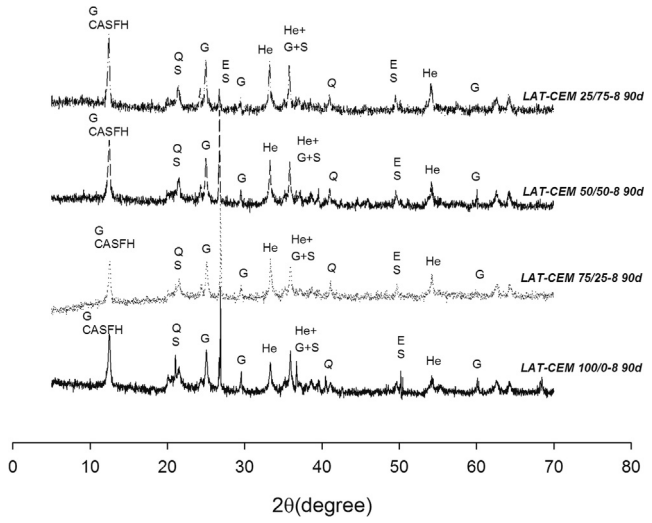

Fig. 3. XRD patterns of different formulations with 8 wt% of cement content at 90 days.

the alkalinity of cement make it evident that most of the mineral phases formed will have iron cations into their structures.

In the laterite, goethite should be present into two forms: amorphous and crystalline. The amorphous fraction is the one participates to the cementitious reactions while the residual goethite (crystalline fraction) transformed to hematite as indicated in the equation (5).

The means phases obtained (gismondine and stratlingite) appear as dominant cementitious phase as from 90 days curing. Phases known for their action regarding the mechanical performance and long-term durability of the cement-based composites. Results significatively different from what has been achieved in the literature up to date (Jaritngam et al., 2014; Obonyo et al., 2014; Millogo et al., 2008; Bouras et al., 2020). The achievement of the results of this work comes from the appropriate selection of the grade of laterite (kaolinite completely corroded) with the fine particles presenting up to 2000 cm^2/g of BET surface area.

The more the laterite-cement composite contains fines, the mores the reflection peaks corresponding to the formation of gismondine and stratlingite compound increase. This can be justified by two ways: firstly, it is known that the fines particles give an easy and quick access to all reactive elements. So, it is possible that a part of the iron contained in the fine particles has reacted immediately in contact with cement and water to form phases like ferrites and another part is transformed to hematite. In coarse particles, to have a complete reaction, it takes time because there is a certain distance between the surrounding of particles and its core; coasres particles that are mainly crystalline. These two reasons could be an explanation to why gismondine, stratlingite and C-A-S-F-H increased with time because at the beginning, the quantity of iron is the same for all specimens.

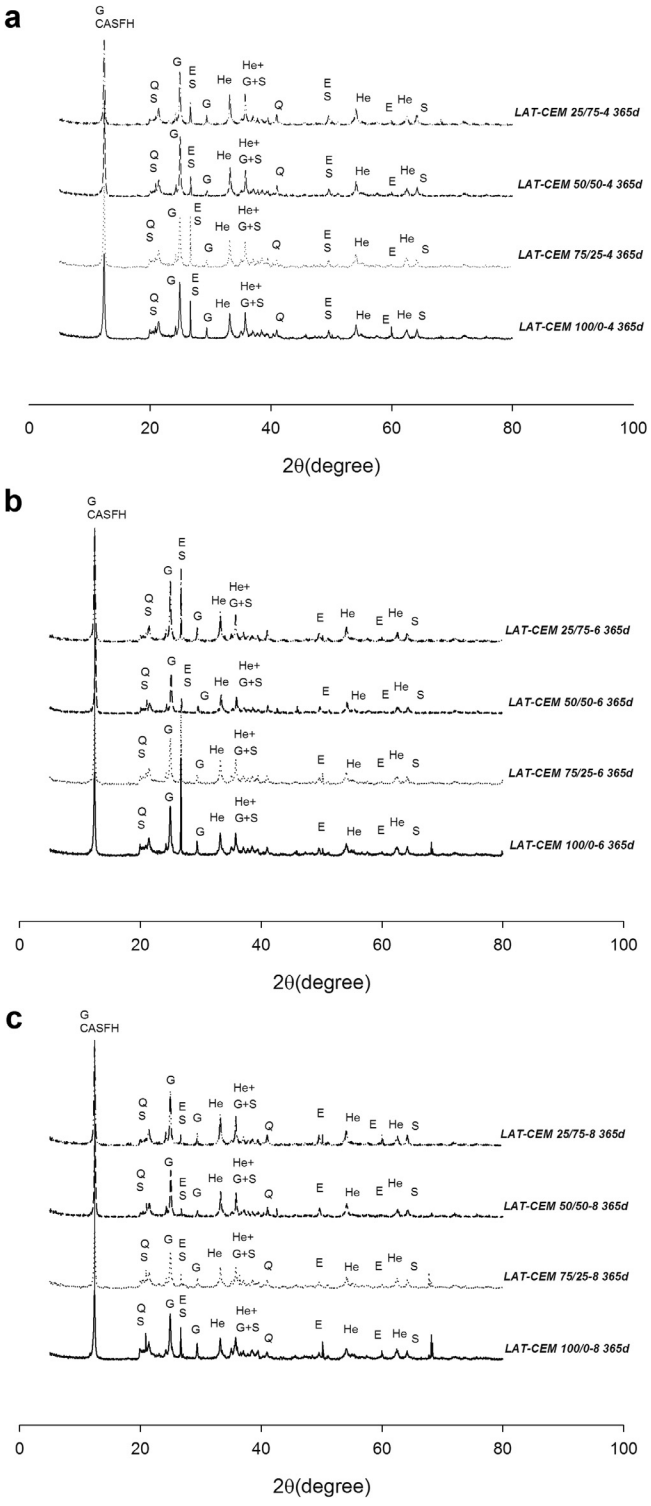

Fig. 4. XRD patterns of different formulations at 365 days with cement content addition: (a) 4 wt%, (b) 6 wt% and (c) 8 wt%.

At 365 days, the minerals phases identified at 90 days remained including gismondine, stratlingite, hematite, quartz and C-A-S-F-H (Fig. 4a, 4b and 4c). During the curing and with the use of laterite containing high amount of iron, the pozzolanic reactions took place in the presence of hydrated cement. Those reactions are completed only within 90 days. Furthermore, the granulometry used for the mix has influence on the formation of cementitious phases justifying the high intensities of the peaks corresponding to gismondine and C-A-S-F-H in the diffractograms of specimens containing fine particles. On the Fig. 2, the XRD patterns related to laterite-cement 100/0–8 at 90 days and 365 days show similar phases although their intensities are different. At 365 days, matrices seem more crystalline than those at 90 days indicating continuous polycondensation through pozzolanic reaction. There are still amorphous or metastable phases which continue to react after 90 days until 365 days, to increase the volume of cementitious phases already described. As confirmed with FT-IR spectra, residues of cement are still present in the matrix after 90 days. Those pozzolanic materials maintain the reactivity of the matrix.

Bulk density, apparent porosity, water absorption and Mercury Intrusion Porosimetry of laterite-cement composites

The specimens with only 2 wt% of cement disintegrated into water indicating that this amount of cement was not enough to produce stable LAT-CEM composites. With 4 wt% of cement, the water absorption varied from 17.90% for the LAT-CEM 100/0 to 14.90% for the LAT-CEM 25/75. It appeared that the ability of the samples to absorb water directly depends to the fines content. From 17.90% for LAT-CEM 100/0, the water absorption decreases to 17.00% for LAT-CEM 75/25; 15.80% for LAT-CEM 50/50 and 14.90% for LAT-CEM 25/75. This decrease of the water absorption is directly linked in the same order to the decrease of apparent porosity and the increase of bulk density (Fig. 6a and 6b). Increasing the cement content to 6 wt%, the decrease in water absorption is significant with the specimens LAT-CEM 100/0 and LAT-CEM 75/25: from 17,90 to 17.30% and 17.00 to 16.00% respectively. The water absorption of specimens LAT-CEM 50/50 and LAT-CEM 25/75 did not change significantly (Fig. 5). Similar behaviour is observed for the two specimens when 8 wt% of cement is added. In the meantime, water absorption of the specimens LAT-CEM 100/0 and LAT-CEM 75/25 continue to decrease suggesting the hypothesis that the ability of the laterite-cement composites to absorb water is linked not only to the level of reaction and formation of C-A-S-F-H phases but also to the fines content (Kasthurba et al., 2008; Kasthurba et al., 2007). In fact, coarse particles of laterites might have shown low sensibility to water while the formation of cementitious phases with fine particles of laterites conducts to matrix more sensible to moisture. This may justify the difference in behaviour between LAT-CEM 100/0 and LAT-CEM 75/25 in the one hand and LAT-CEM 50/50 and LAT-CEM 25/75 in the other hand. Behaviour that corroborate with the variation of the apparent density and the continuous increase in densification with the coarse particle content (Fig. 6a and 6b).

From the cumulative pore volume and pore size distribution curves (Fig. 7a and 7b), LAT-CEM 100/0 is dominated by nanopores (pore size between 0.01 and 0.1 μm) and presents relatively low volumes of pores between 0,1 and 1 μm together with those of the bands centred at 10 μm. The nanoporosity with the principal band described here is typically that of cementitious materials (Zhao et al., 2014; Shi and Brown, 1991; Ma, 2014). Conventionally, with C-A-S-H or C-A-S-F-H, the nanopores have band that are monomodal as it is visible with the cumulative pore volume of LAT-CEM 100/0. In the case of this work, as can be observed into the Fig. 7a, the nanopores are not the only class of porosity due to the fact that the fine fractions of laterites still have some unreacted particle as demonstrated by the granulometry in Table 3 (~15 wt% of $\phi \leq 2$ μm; ~ 27.6 wt% of 2 μm $\leq \phi \leq$ 10 μm and ~ 58 wt% of 10 μm $\leq \phi \leq$ 1 mm) and ESEM. Coarse particles that induce the micrometrics porosity. With the increase of the fraction of coarse particles, it can be observed an increase of the bands of pores situated in the region between 0.1 and 1 μm as those centred at 10 μm. The augmentation of the coarse fraction increased the interface between cementitious materials and aggregates. This trend is confirmed with the increase of the coarse porosity with almost complete reduction of the nanopores in to the specimen LAT-CEM 50/50 and LAT-CEM 25/75. In the Fig. 5, it is

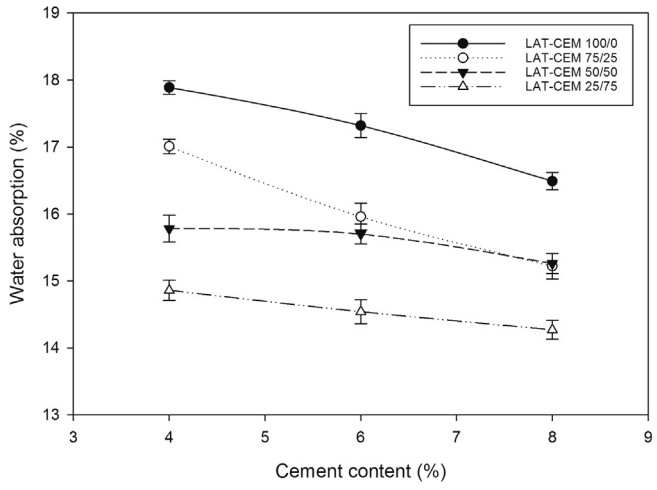

Fig. 5. Water absorption behaviour of laterite-cement composites.

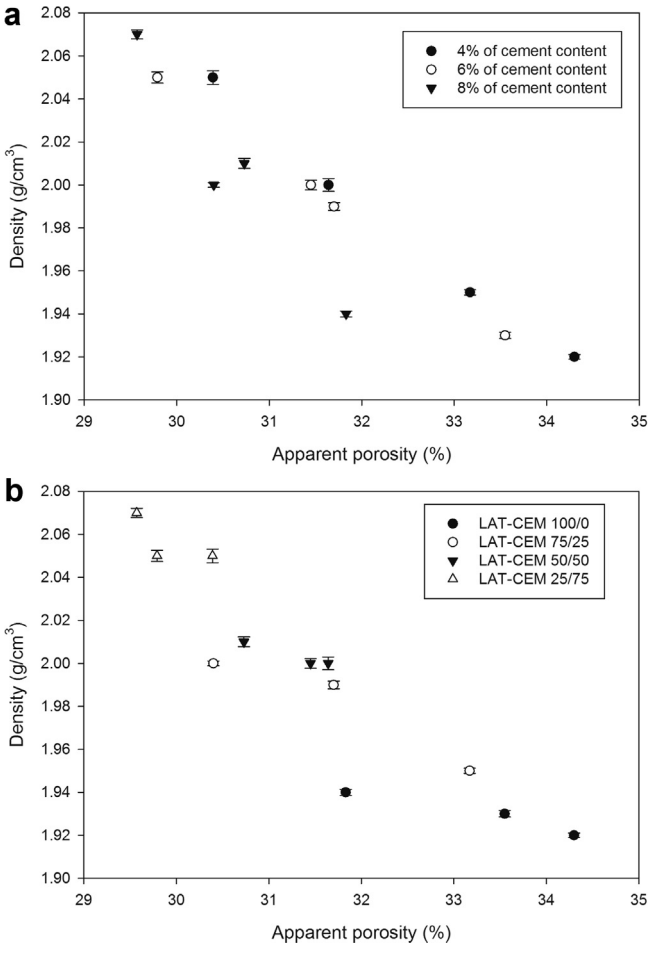

Fig. 6. Correlation between bulk density and total porosity: (a) function of cement content and (b) function of particles size distribution.

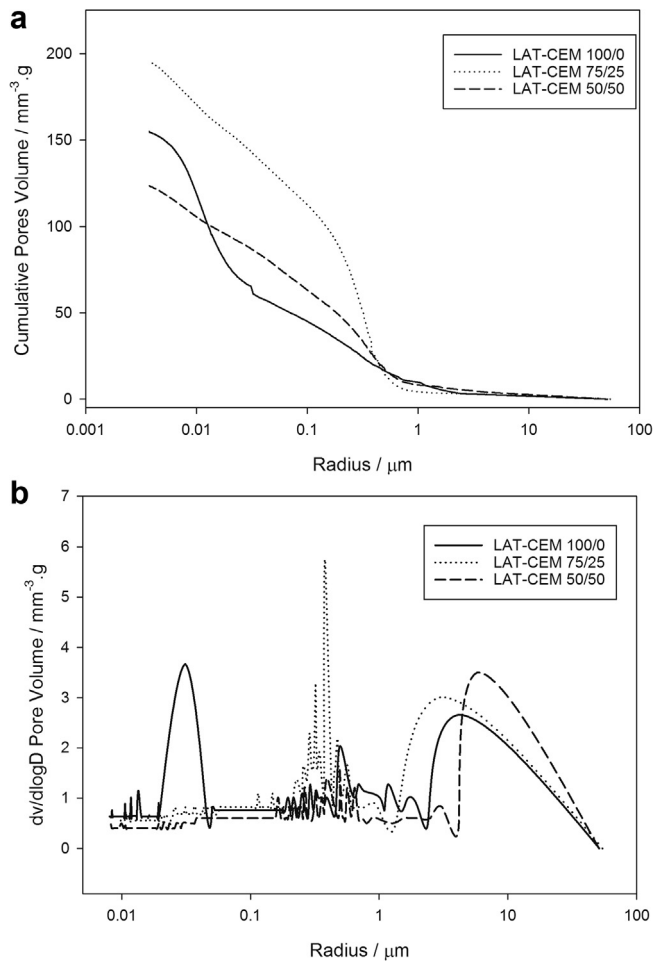

Fig. 7. (a) Cumulative pore volume and (b) variation of pore size distribution for laterite-cement composites.

observed that the volume of water absorption decreases with the increase of the coarse particles. In regard with the pore size distribution and the cumulative pore volume, it should be noted that the fraction of water absorbed during immersion might remain into the microstructure and explains partly the relatively high values of water absorption of the samples LAT-CEM 100/0. In fact, during immersion that takes 24 h, the water molecules have enough time to penetrate and saturate those nanopores (El-Diadamony et al., 2018; Zhou et al., 2010). However as demonstrated by Kamseu and co-workers (Kamseu et al., 2018), the molecules of water present into those nanopores cannot be desorbed instantaneously as those from capillary pores. Their desorption is time–temperature dependent and cannot be effective within the cycle of time provided with the experimental method regarding the water absorption test.

Physico-mechanical properties

Fig. 8 shows the variation of the linear shrinkage as function of the particles size distribution and the cement content. It is observed that the LAT-CEM 100/0 exhibits the high linear shrinkage (3.2%) whatever is the cement content. With 25% of coarse laterite (LAT-CEM 75/25), the linear shrinkage drops under 3% apart from the specimen with 2 wt% of cement where one can notice a poor level of reactivity. Increasing the coarse particles, the general behaviour is the constant value of linear shrinkage of 2.8% for 2 and 4 wt% of cement while with 6 and 8 wt%, the linear shrinkage is stable at 2.1%. These results allow to establish the suggestion that between 2 and 4 wt% of cement, the reaction laterite-cement is not optimal in the matrix. Residual and non-reacted clayey material responsible for the relativity high linear shrinkage are still present. At 6 wt% of cement, the value of linear shrinkage obtained seems to be appropriate as the extend of cement content to 8 wt% did not modify the linear shrinkage. Moreover, as demonstrated with XRD analysis and IR patterns, residual C-S-H was observed in the sample with 8 wt% of cement content suggesting that the value of 6 wt% of cement should be the optimum. In fact, as pozzolanic material, laterite should react with cement in hydration condition to form news phases (C-A-S-F and C-A-S-F-H). The presence of hydrated phase (C-S-H) in laterite cement composite, should be interpreted as residual material. In this composite, C-S-H is an intermediate product which presence at the end of the curing implied the unavailability of pozzolan (laterite). The kaolinite contained in laterite being metastable suggests the reactivity of all its elements such as iron, silicon and aluminium with the hydrated cement, which will favour the formation of the CSH and CASFH phases. However, part of the silica coming from the quartz and the iron hydrates will not react but will behave as micro aggregates and reinforce the matrix. The relative high value of linear shrinkage is also justified by the low level of porosity and pore size as indicated in Fig. 4 for LAT-CEM 100/0 while the reduction of linear shrinkage in the sample containing high proportions of coarse laterite is correlated with important capillary porosity (larger pores).

High values of shrinkage of LAT-CEM 100/0 and LAT-CEM 75/25 correspond into the Fig. 9a to high values of flexural strength while low value of shrinkage of LAT-CEM 50/50 and LAT-CEM 25/75 correspond to low values of flexural strength. In fact, LAT-CEM 100/0 and LAT-CEM 75/25 presented the value of 4, 7, 10 and 11 MPa respectively for 2, 4, 6 and 8 wt% of cement. In both formulations, the content of fines is high and the mix with cement directly conduct to the formation of cementitious materials (chemicals bounding) responsible for the flexural strength. With the reduction of fine content (LAT-CEM 50/50 and LAT-CEM 25/75) the flexural strength decreases as the level of reactions decrease because the coarse particles reduce the extend of cementitious phases responsible for the bonding strength. In both formulations, the addition of 2 wt% of cement maintains the flexural strength under 4 MPa. From 4 wt% of cement, the value obtained (between 4 and 7 MPa) are those generally obtained with standard mortars and concrete (Mulyadi, 2017). The variations of the compressive strength of laterite cement composite are summarized into the Fig. 9b. It appears that the specimen of LAT-CEM 100/0 and LAT-CEM 75/25 with high fines content, although their relatively high values of flexural strength, present low values of compressive strength compared to the formulations of LAT-CEM 50/50 and LAT-CEM 25/75. The compressive strength seems to be affected by the particles size distribution than to the reactivity. The combination of fine and coarse particles contributes to improve the packing behaviour by the way the compressive strength. For a similar value of cement content, the combination of LAT-CEM 50/50 or LAT-CEM 25/75 seems more

Table 3
Cumulative volume of Particle of laterite passing at different sizes of sieve.

	Φ ≤ 2 µm	Φ ≤ 10 µm	Φ ≤ 25 µm	Φ ≤ 100 µm	Φ ≤ 1000 µm
Laterite	15.02	42.91	62.13	89.40	100
Cement	10.88	50.65	100	100	100

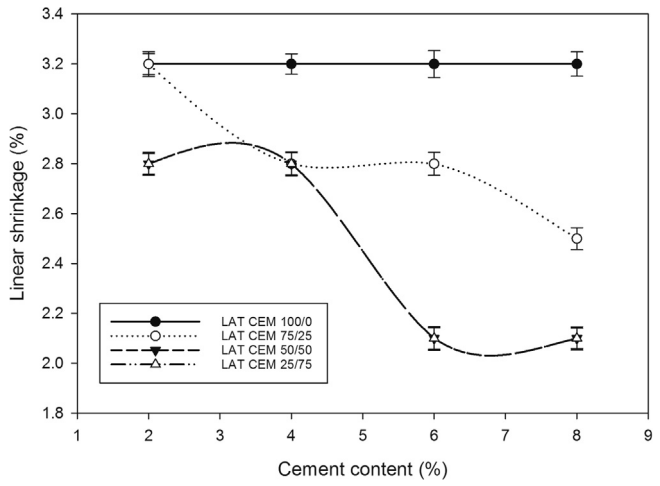

Fig. 8. Variation of the linear shrinkage of different composition as function of cement content.

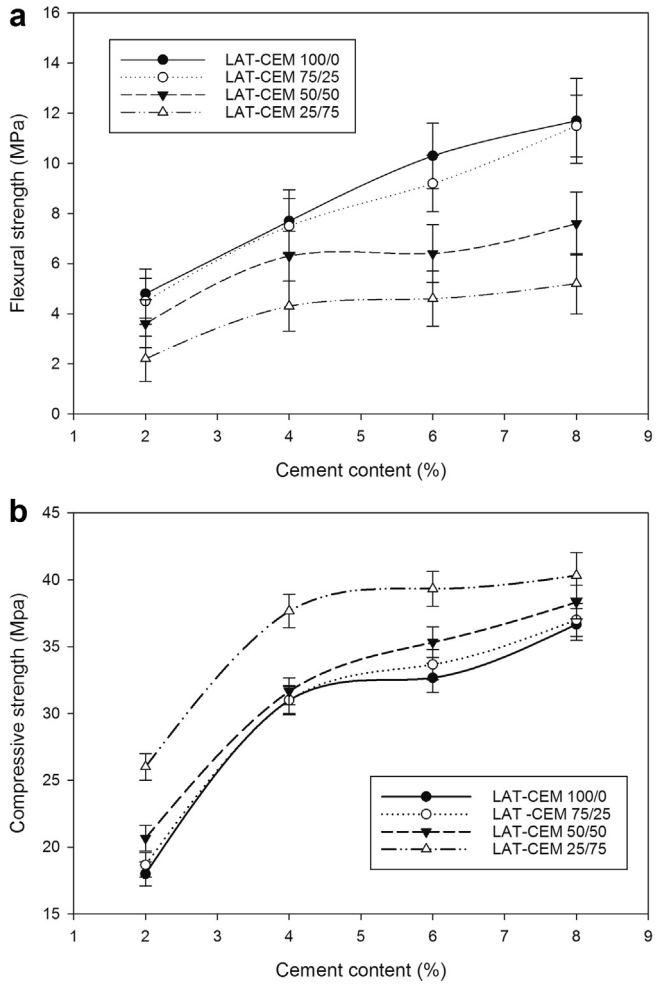

Fig. 9. Mechanical properties as function of cement content (a) Flexural strength and (b) Compressive strength.

benefit for the achievement of higher compressive strength compared to the formulations dominated by fine (LAT-CEM 100/0 and LAT-CEM 75/25) (Fig. 9b). While the compressive strength of formulations dominated by coarse particles were respectively 23 and 27 MPa, those dominated with fines presented compressive strength under 20 MPa although their relatively high flexural strength. So, in the point of view of standards, the formulations with coarse particles containing the same value of 2 wt% of cement are conformed with the standard CIP 35-Testing compressive strength of concrete while those dominated by fine are not conform. Increasing the cement content to 4, 6 or 8 wt%, the value of compressive strength was above 30 MPa whatever the particles size distribution considered. The formulation LAT-CEM 25/75 even give value of compressive strength above 40 MPa when a minimum of 6 wt% of cement is applied. Globally, as already suggested with XRD and IR spectra, optimum LAT-CEM composites can be achieved with 6 wt% of cement and a combination of fines and coarse LAT-CEM particles in the range of 50/50 and 25/75. These combinations are capable to develop enough amount of gismondine and stratlingite together with C-A-S-F-H phases that ensure optimum densification and compactness in a context of an optimum particles packing.

Microstructure of laterite-cement composite

Fig. 10 presents the micrographs of the LAT-CEM 100/0 at 1 day at low magnification. It can be observed a homogenous microstructure with some pores (Fig. 10a). This proves that fine particles size of LAT-CEM 100/0 permit to achieve a good reactivity and cohesion between the particles and phases formed. But, one can also observe the residual particles of laterite. In fact, at this level of curing (1 day), the reactions between the cement and the laterite are just starting. And low compactness observed on this specimen is due to the amount of portlandite within matrices which are still to be consumed. This trend is in agreement with the phase's evolution (Figs. 1 and 2). On the Fig. 10a, the round pores are voids from the sites previously occupied by water. This water which is from the preparation of specimens evaporate during curing and produces large pores. On the Fig. 11, there are micrographs of specimens cured at 90 days (lower magnification). According to these figures, there was not a real difference in term of densification between LAT-CEM 100/0 and LAT-CEM 75/25 indicating that laterite particles are well bounded by the reacted phases sufficiently cover the grain particles of the matrices. LAT-CEM 50/50 show microstructure less compact and less homogenous. That is why the flexural strength of LAT-CEM 100/0 and LAT-CEM 75/25 are higher. The reactions being sufficiently efficient and complete, produce enough binder compared to the LAT-CEM 50/50. This is due to its coarse particles which make that the bending phases developed can't embed the matrices enough. In those specimens, the cementitious phases from the reaction between laterite and cement seem to be not enough to cover the coarse grains as it is case in LAT-CEM 100/0 and LAT-CEM 75/25. This situation is responsible for the increase of porosity and pores size. In contact with cement, fines grains powder of laterite reacts in presence of water to form phase like gismondine and stratlingite together with C-A-S-H and C-A-S-F-H. This induces a good combination of the cementitious phases with coarse grains improving mechanicals strength as from the high cohesion and particle packing when the fine/coarse ratio is appropriate.

At high magnification (Fig. 12), it seems that it is obviously difficult only with ESEM to identify the phases formed. For this reason, a semi quantitative EDX analysis at 03 points was done on a sample as shown in Fig. 13. It was noticed that elements such as iron, Al, Si, 0 and Ca are in the majority next to some impurities like Titanium grains (represented by the lightening zones on micrographs). It can therefore be concluded that these elements are involved in the formation of the cementitious phases such as CASH and CASFH where it can be found gismondine, stratlingite, etc…, exactly as found with XRD and IR analysis. In the domains containing C-A-S-H and C-A-S-F-H the iron phase is less present (Fig. 12b) and becomes more visible in Fig. 12c. These observations can signify that the coarse particles do not react completely and the reaction took place just at the surface of the particles.

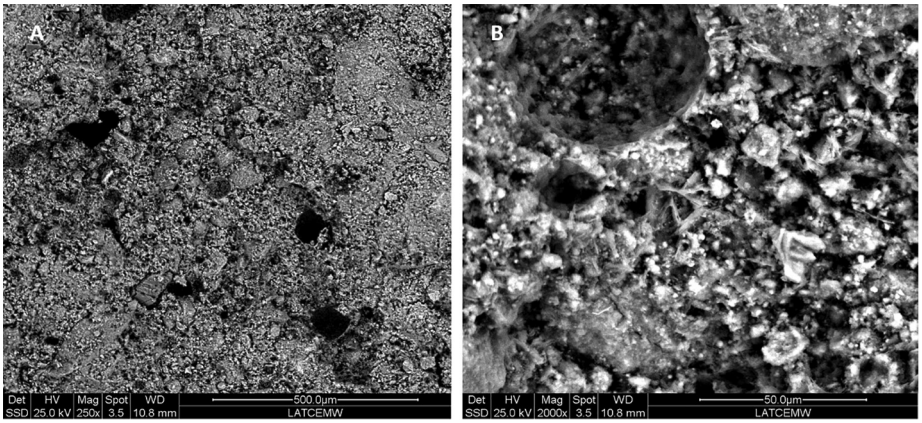

Fig. 10. SEM Micrographs of LAT-CEM 100/0 at 1 day.

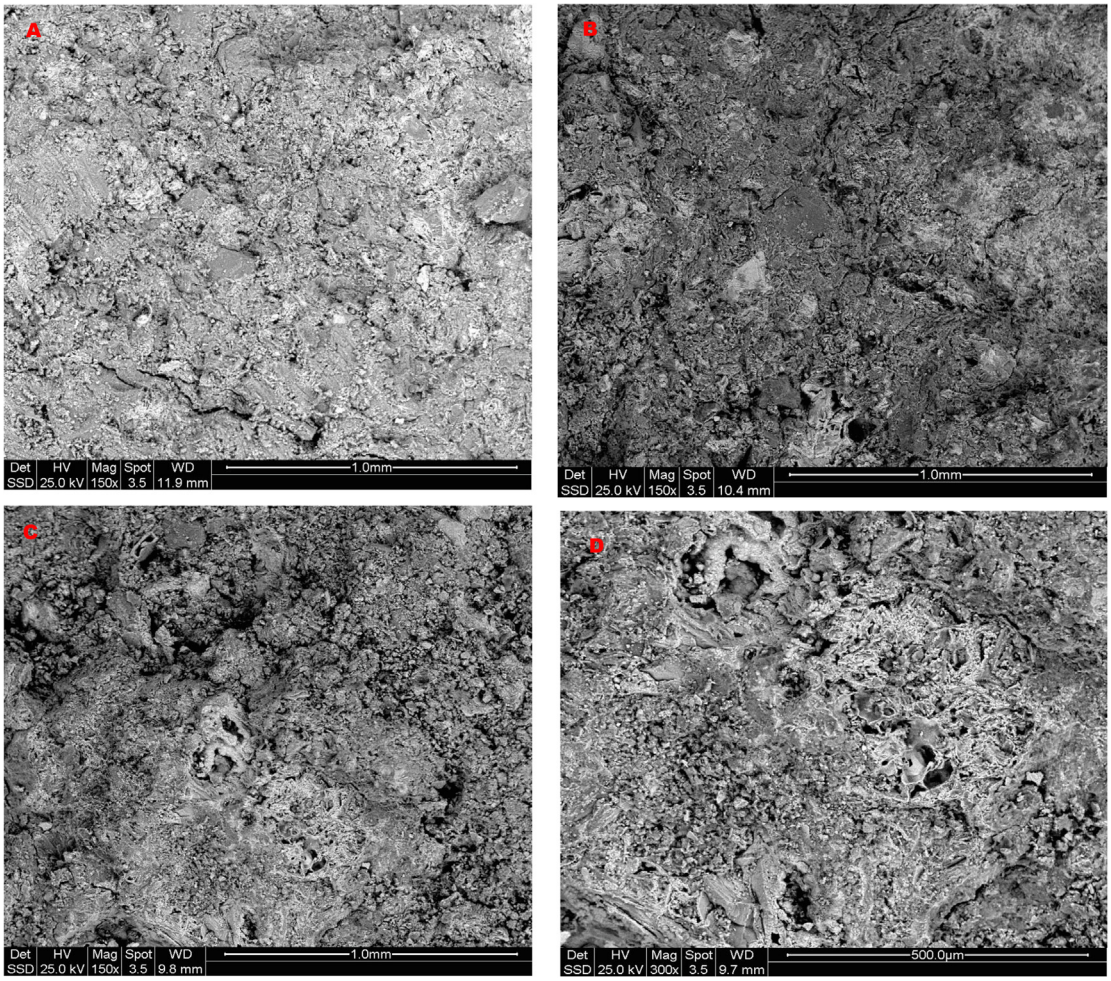

Fig. 11. SEM Micrographs of laterite-composite (a) of LAT-CEM 100/0, (b) of LAT-CEM 75/25, (c) of LAT-CEM 50/50 and (d) of LAT-CEM 25/75 at 90 days at low magnification.

That is why the flexural strength of laterite containing coarse particles is low compared to those with more fines (Fig. 9a). However, knowing that coarse particles of laterites are responsible for the high compressive strength, the relatively poor reactivity of LAT-CEM 50/50 and LAT-CEM 25/75 did not affect negatively the values of compressive strength. Nevertheless, the increase of coarse particles increases the compressive strength as a good combination of reactive phases with fine particles that embed the coarse efficiently when the fine/coarse ratio is appropriate. The difference on the morphology (Fig. 12d) explains the diversity of phases formed into the specimens. This assertion get clarification with Fig. 13 when one can see on the same specimen two different phases (C-A-S-H and C-A-S-F-H) with three scales of sizes. C-A-S-F-H is dominated by iron while calcium is very low, another phase shows a decrease of iron and increase of calcium and

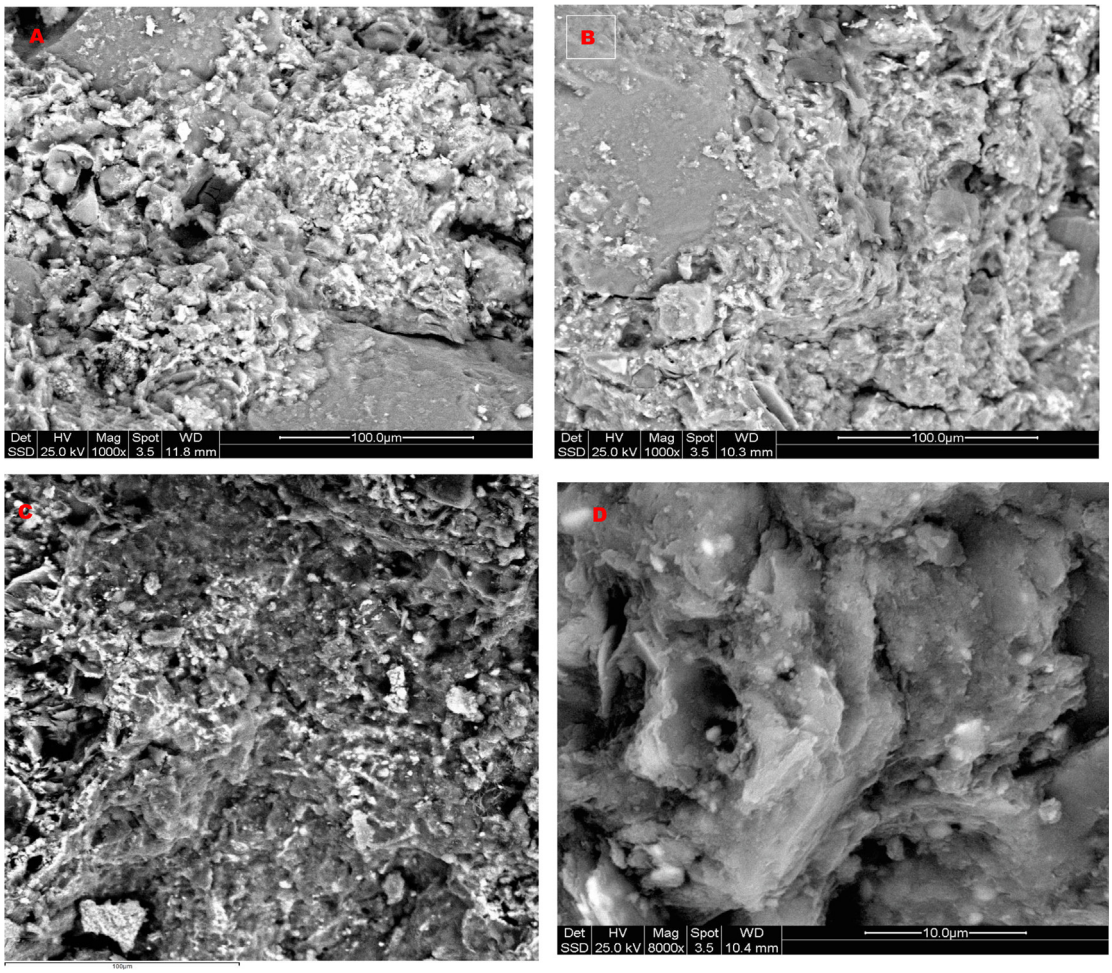

Fig. 12. SEM Micrograph of laterite-composite (a) of LAT-CEM 100/0, (b) of LAT-CEM 75/25, (c) of LAT-CEM 50/50 and (d) of LAT-CEM 25/75at 90 days at high magnification.

the last has morphology with a high corrosion due to the iron. In each matrix, silica and alumina are well represented justifying the fact that, in the specimen studied, the binder phases are constituted by iron-rich calcium aluminosilicates. The binder phase is responsible for the densification and compactness of the laterite-cement composites systems.

Discussions

Laterite is formed from the corrosion of kaolinite by iron minerals (Fe^{2+} and Fe^{3+}based minerals). The iron cations replace the aluminium in octahedral sites, substitution that affects the crystalline structure. The substitution transforms the kaolinite minerals to semi-amorphous leading to the vulnerability of the solid precursor to chemical attack particularly in alkaline media. The main residue of the hydration of cement ($Ca(OH)_2$) reacts with SiO_2, Al_2O_3 and Fe_2O_3 (γ-FeOOH) species of disordered structure of laterite. These reactions form additional binding phases such as C-A-S-H and C-A-F-S-H responsible for the good cohesion between different particles within the matrices. These binding phases depend on the degree of corrosion of the kaolinite justifying the significant role of iron and chemical composition in mechanical and microstructural improvement. The formation of Gismondine, stratlingite and others iron-rich cementitious phases in addition to ettringite demonstrated that laterite is a natural solid precursor prompt to combine with C-S-H and CH without any pretreatment. It is green, energy-efficient and sustainable raw materials for future environment as nowadays extensive research is conducted seeking green binders and green raw materials for sustainable building and construction.

With regard to particle size, it was found that the finer the particles are, more compact and denser the final product is, which has a positive impact on bending strength. Coarse particles, on the other hand improve the compressive strength of the material. The coarser the particles more resistant the compressive strength. Hence, the size of the particles has a significant impact on the mechanical and microstructural properties. The structural disorder due to the corrosion of the kaolinite, the iron substitution and the particles size were found as key parameters governing the mechanical and microstructural properties of laterite-cement composites. The goethite and others oxyhydrates present are capable to react in alkaline media allowing the iron cations to participate has ion former. Those that do not participate are transformed to stable phase of hematite.

It is important to notice that a stabilization with 2 wt% of cement presents values of flexural and compressive strength very low and far from those stabilized with 4, 6 and 8 wt% indicating that 2 wt% cannot be used to achieve good laterite-cement composites. The granulometry and the nature of laterite regarding the mineralogical composition are not the only factors that influence the properties of laterite-cement composites. The cement content also has an important role in terms of the degree of cohesion between the particles. In fact, cement content in the range 4–6 wt% is significant to achieve enough cementing agents and more reactions with the disordered and amor-

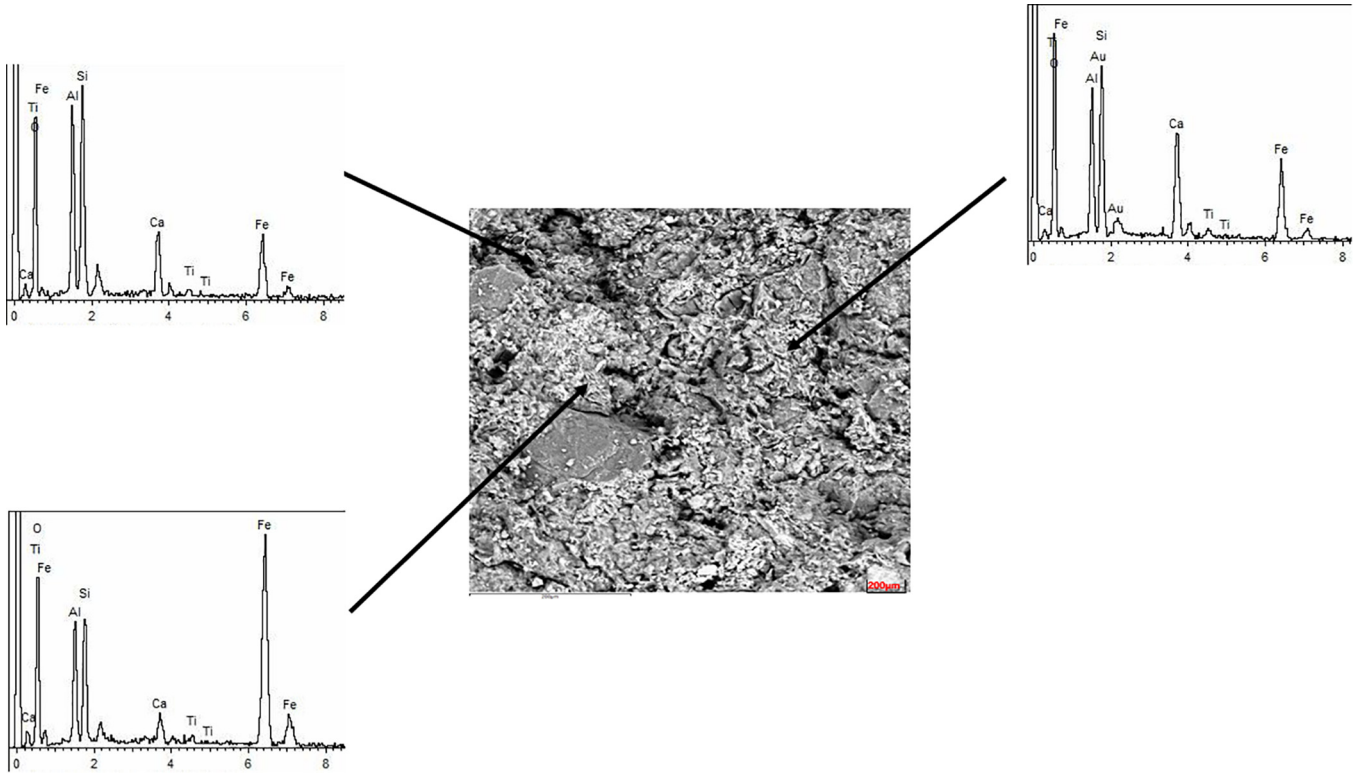

Fig. 13. SEM-EDS spectrum of LAT-CEM 100/0 at 90 days.

phous components of the laterite. The increase of the cement content, from 4 to 6 wt% in a matrix with well-designed granulometry conducts to an optimum microstructure for the lower porosity and water absorption (Figs. 5 and 6). Since the major part of reactions took place already at 90 days and just a small residual fraction is transformed between 90 and 365 days, 90 days could be considered as maximum curing period. However, as the minimum strength required is achieved as from 28 days, the laterite-cement composites seem to fulfil the requirements of the standards when consider the building materials.

The Fig. 14 shows the relationship between compressive and flexural strengths as function of the cement content and particles size distribution. A carefully interpretation of this figure let observe correlation between the flexural and compressive strengths: the correlation coefficient in the cases of LAT-CEM 100/0 and LAT-CEM 25/75 is 0.72. However, when there is a good combination between fine and coarse particles, the correlation's coefficient between the flexural and compressive strength reaches 0,85. It appears that the mineralogy, particles size distribution and optimization of the reactivity present laterite-cement composites with very good performances. Due to the large availability of the laterites in tropical area of world and the relatively low amount of cement needed for the composite design, it is possible to produce laterite-cement composite locally. The process is relatively economic in terms of the energy linked to the transport of raw material in comparison for the transport of aggregate and sand, as well as the energy of grinding which is considerably low with respect to energy to ground the aggregate.

Several authors evaluated both energies from the transport of raw material to their transformation and found that laterite-cement composite required 50 to 100 kWh/m^3 whereas concrete needed 400 to 800 kWh/m^3 (Meukam et al., 2003; Damfeu, 2016). Concerning carbon emission, blocks made with laterite create 222 kg CO_2/tonne compare to that of concrete blocks (800–1000 kg CO_2/tonne) (Fernandez et al., 2011; Forster et al., 2020; Waziri et al., 2013). Moreover, laterite cement composite matrix presents low thermal conductivity allowing the possibility to achieve thermal comfort (19–22 °C) throughout the year without soliciting electric air conditioner. This means significant safe of energy in comparison with cement-sand-aggregate block that have high thermal conductivity and need the use of electric air conditioner to have thermal comfort because of their high capacity to accumulate heat.

In the tropical area, it is easier to have laterite as raw material for the development of structural matrix for building and construction than to have plastic and fusible clay generally use for ceramics products. The industrial applications of those type of composite is evidently bricks for building, pavement, etc.

The innovative approach appears efficient and viable solution for the development of eco-friendly composites for sustainable building solutions.

Conclusions

Laterite with high level of corrosion of kaolinite by iron minerals (≥37.5 of Fe_2O_3 + FeO) was used for the design of laterite-cement composites. Concretions collected were dried (using solar drying) and ground to have different grade of granulometry. The powder obtained received 2, 4, 6 and 8 wt% of cement Portland type CEM II 42.5. The analysis and characterisations of the final products allowed to draw the following conclusions:

- Laterite with high level of corrosion of kaolinite by iron effectively demonstrated good reactivity with cement with almost complete conversion of the iron-rich aluminosilicates to cementitious phases: gismondine, stratlingite in addition to C-A-S-H and C-A-S-F-H.
- The combination of fine ($\phi \leq 1$ mm including nano and micro particles) and coarse particles (1 mm $\leq \phi \leq$ 4 mm) permitted to develop better packing process with the fine particles that form cementitious binders capable to densify the matrices to low water absorption range.

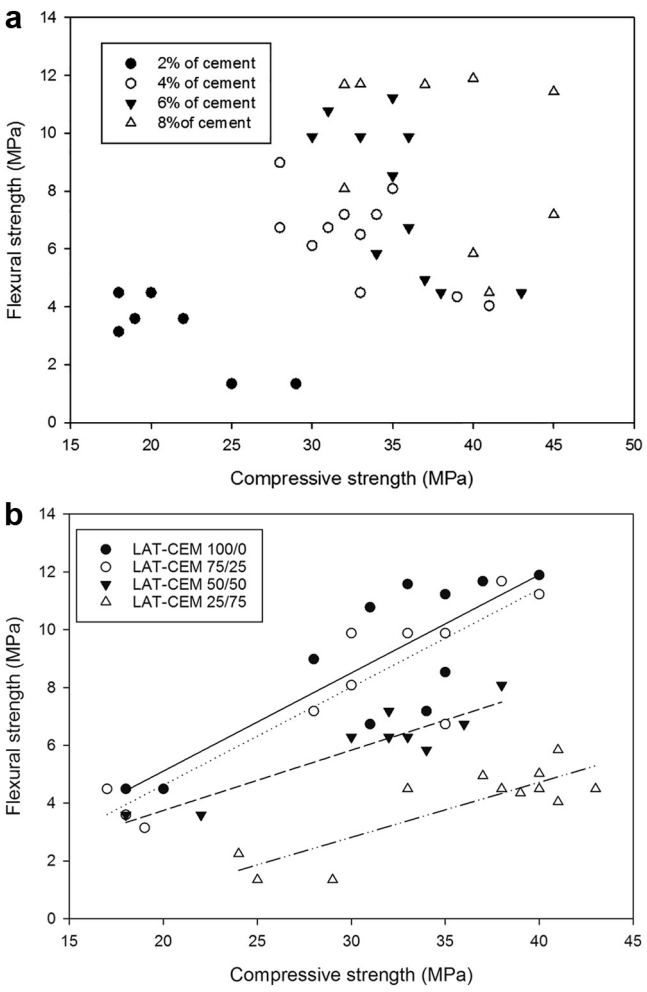

Fig. 14. Correlation between compressive strength and flexural strength respectively as (a) function of cement content and (b) particles size distribution.

- C-A-S-H and C-A-S-F-H contributed to compact the microstructure with significantly improve of the flexural and compressive strengths.
- The flexural strength (~12 MPa) and compressive strength (~40 MPa) achieved let the laterite-cement composites appeared innovative and significant contribution for this new material classified as green and sustainable in regard to the large availability of laterites in tropical area and the very low amount of binder (4–6 wt%) needed.
- The laterites used in this study could be used as "green metakaolin", ideal natural solid precursor for energy-efficient and sustainable binder and composite.
- Bricks with high flexural strength can be used as facing bricks while those with high compressive strength can be used as structural bricks.

CRediT authorship contribution statement

Van Essa L.K. Samen: Conceptualization, Methodology, Investigation, Writing – original draft. **Rodrigue Cyriaque Kaze:** Validation, Writing - review & editing, Visualization. **Juvenal Giogetti N. Deutou:** Validation, Methodology, Writing - review & editing, Visualization. **H.K. Tchakoute:** Methodology, Writing - review & editing. **P. Meukam:** . **E. Kamseu:** Supervision, Methodology, Resources. **C. Leonelli:** Resources, Supervision.

Declaration of Competing Interest

The authors declare that they have no known competing financial interests or personal relationships that could have appeared to influence the work reported in this paper.

Acknowledgements

The authors of this article wish to acknowledge the FLAIR Fellowship African Academic of Science and the Royal Society. No. FLR/R1/201402.They also acknowledge the support of the French University Agency through the grant to Elie Kamseu. Some of the analysis and characterization of this paper were possible with the financement.

Compliance with ethical standards

This manuscript has been published elsewhere in any form or language and has not been submitted to more than one journal for simultaneous consideration.

References

A. Alujas, R.S. Almenares, S. Betancourt, C. Leyva, Pozzolanic reactivity of low grade kaolinitic clays: Influence of mineralogical composition, 2015. https://doi.org/10.1007/978-94-017-9939-3_42.

ASTM C39/C39M - 05, Standard Test Method for Compressive Strength of Cylindrical Concrete Specimens, ASTM Int. (2005) 1–8. https://doi.org/10.1520/C0039.

Astm C78/C78M - 02:, Astm C78/C78M - 02:, Stand. Test Method Flexural Strength Concr. (Using Simple Beam with Third-Point Loading)ASTM Int. USA. 04.02 (2002) 1–3. https://doi.org/10.1520/C0078_C0078M-16.

Awoyera, P.O., Akinmusuru, J.O., Dawson, A.R., Ndambuki, J.M., Thom, N.H., 2018. Microstructural characteristics, porosity and strength development in ceramic-laterized concrete. Cem. Concr. Compos. 86, 224–237. https://doi.org/10.1016/j.cemconcomp.2017.11.017.

Billong, N., Melo, U.C., Louvet, F., Njopwouo, D., 2009. Properties of compressed lateritic soil stabilized with a burnt clay-lime binder: Effect of mixture components. Constr. Build. Mater. 23, 2457–2460. https://doi.org/10.1016/j.conbuildmat.2008.09.017.

B.F. Bouras, N. Tapsoba, M. Martin, S. Sabio, A. Jacquet, K. Beck, N. Belayachi, M. Bouasker, M. Al-mukhtar, Effect of Hydrated Lime and Cement on the Engineering Behavior of Highly Expansive Clay, 7 (2020) 1–14.

C. ASTM, Standard Test Method for Water Absorption , Bulk Density, Apparent Porosity, and Apparent Specific Gravity of Fired Whiteware Products 1, 88 (2008) 14–15.

Changling, H., 1969. Analysis of double-beam parametric amplifier. Cem. Concr. Res. 14, 666–674. https://doi.org/10.1016/0008-8846(95)00165-4.

Damfeu, C., 2016. Caracterisation thermophysiques des materiaux locaux d'isolation thermique de batiment et modelistion des transferts thermiques 1. These, 1–215.

Djobo, J.N.Y., Elimbi, A., Tchakouté, H.K., Kumar, S., 2017. Volcanic ash-based geopolymer cements/concretes: the current state of the art and perspectives. Environ. Sci. Pollut. Res. 24, 4433–4446. https://doi.org/10.1007/s11356-016-8230-8.

El-Diadamony, H., Amer, A.A., Sokkary, T.M., El-Hoseny, S., 2018. Hydration and characteristics of metakaolin pozzolanic cement pastes. HBRC J. 14, 150–158. https://doi.org/10.1016/j.hbrcj.2015.05.005.

Fernandez, R., Martirena, F., Scrivener, K.L., 2011. The origin of the pozzolanic activity of calcined clay minerals: A comparison between kaolinite, illite and montmorillonite. Cem. Concr. Res. 41 (1), 113–122. https://doi.org/10.1016/j.cemconres.2010.09.013.

Forster, A.M., Válek, J., Hughes, J.J., Pilcher, N., 2020. Lime binders for the repair of historic buildings: Considerations for CO2 abatement. J. Clean. Prod. 252, 119802. https://doi.org/10.1016/j.jclepro.2019.119802.

Horgnies, M., Chen, J.J., Bouillon, C., 2013. Overview about the use of fourier transform infrared spectroscopy to study cementitious materials. WIT Trans. Eng. Sci. 77, 251–262. https://doi.org/10.2495/MC130221.

Jaritngam, S., Prachasaree, W., Somchainuek, O., Taneerananon, P., 2012. An investigation of lateritic soil cement for sustainable pavements. Indian J. Sci. Technol. 5, 3603–3606.

Jaritngam, S., Yandell, W.O., Taneerananon, P., 2013. Development of strength model of lateritic soil-cement. Eng. J. 17, 69–78. https://doi.org/10.4186/ej.2013.17.1.69.

Jaritngam, S., Somchainuek, O., Taneerananon, P., 2014. Feasibility of laterite-cement mixture as pavement base course aggregate. Iran. J. Sci. Technol. - Trans Civ. Eng. 38, 275–284.

Jean Noël, Y., Djobo, A., Elimbi, D.S., 2020. Phase and dimensional stability of volcanic ash - based phosphate inorganic polymers at elevated temperatures. SN Appl. Sci., 828. https://doi.org/10.1007/s42452-020-2616-4.

Kamseu, E., Lancellotti, I., Sglavo, V., Modolo, L., Leonelli, C., 2016. Design of inorganic polymer mortar from ferricalsialic and calsialic slags for indoor humidity control. Materials (Basel). 9, 410. https://doi.org/10.3390/ma9060410.

Kamseu, E., Mohamed, H., Sofack, J.C., Chaysuwan, D., Tchakoute, H.K., Djobo, J.N.Y., Rossignol, S., Leonelli, C., 2018. Moisture control capacity of geopolymer composites: correlation of the bulk composition-pore network with the absorption-desorption behavior. Transp. Porous Media. 122, 77–95. https://doi.org/10.1007/s11242-017-0990-1.

Kapeluszna, E., Kotwica, Ł., Różycka, A., Gołek, Ł., 2017. Incorporation of Al in C-A-S-H gels with various Ca/Si and Al/Si ratio: microstructural and structural characteristics with DTA/TG, XRD, FTIR and TEM analysis. Constr. Build. Mater. 155, 643–653. https://doi.org/10.1016/j.conbuildmat.2017.08.091.

Kasthurba, A.K., Santhanam, M., Mathews, M.S., 2007. Investigation of laterite stones for building purpose from Malabar region, Kerala state, SW India - Part 1: Field studies and profile characterisation. Constr. Build. Mater. 21, 73–82. https://doi.org/10.1016/j.conbuildmat.2005.07.006.

Kasthurba, A.K., Santhanam, M., Achyuthan, H., 2008. Investigation of laterite stones for building purpose from Malabar region, Kerala, SW India - Chemical analysis and microstructure studies. Constr. Build. Mater. 22, 2400–2408. https://doi.org/10.1016/j.conbuildmat.2006.12.003.

Kaze, R.C., Beleuk à Moungam, L.M., Fonkwe Djouka, M.L., Nana, A., Kamseu, E., Chinje Melo, U.F., Leonelli, C., 2017. The corrosion of kaolinite by iron minerals and the effects on geopolymerization. Appl. Clay Sci. 138, 48–62. https://doi.org/10.1016/j.clay.2016.12.040.

Kaze, R., Myllyam, L., Cannio, M., Rosa, R., Kamseu, E., Chinje, U., Leonelli, C., 2018. Microstructure and engineering properties of Fe 2 O 3 (FeO) -Al 2 O 3 -SiO 2 based geopolymer composites. J. Clean. Prod. 199, 849–859. https://doi.org/10.1016/j.jclepro.2018.07.171.

Lasisi, F., Osunade, J.A., Adewale, A.O., 1990. Short-term studies on the durability of laterized concrete and laterite-cement mortars. Build. Environ. 25, 77–83.

Latifi, N., Eisazadeh, A., Marto, A., 2014. Strength behavior and microstructural characteristics of tropical laterite soil treated with sodium silicate-based liquid stabilizer. Environ. Earth Sci. 72, 91–98. https://doi.org/10.1007/s12665-013-2939-1.

Leonelli, C., Kamseu, E., Boccaccini, D.N., Melo, U.C., Rizzuti, A., Billong, N., Miselli, P., 2007. Volcanic ash as alternative raw materials for traditional vitrified ceramic products. Adv. Appl. Ceram. 106, 135–141. https://doi.org/10.1179/174367607X159329.

Lucia, M.D., 2011. X-ray diffraction study of hydration processes in the Portland cement. J. AES 1, 79–86. https://doi.org/10.1093/gerona/55.6.B274.

Ma, H., 2014. Mercury intrusion porosimetry in concrete technology: Tips in measurement, pore structure parameter acquisition and application. J. Porous Mater. 21, 207–215. https://doi.org/10.1007/s10934-013-9765-4.

Maddalena, R., Roberts, J.J., Hamilton, A., 2018. Can Portland cement be replaced by low-carbon alternative materials? A study on the thermal properties and carbon emissions of innovative cements. J. Clean. Prod. 186, 933–942. https://doi.org/10.1016/j.jclepro.2018.02.138.

P. Meukam, A. Noumowe, Y. Jannot, R. Duval, Caractérisation thermophysique et mécanique de briques de terre stabilisées en vue de l'isolation thermique de bâtimentThermophysical and mechanical characterization of stabilized clay bricks for building thermal insulation, Mater. Struct. 36 (2003) 453–460. https://doi.org/10.1007/bf02481525.

Millogo, Y., Hajjaji, M., Ouedraogo, R., Gomina, M., 2008. Cement-lateritic gravels mixtures: Microstructure and strength characteristics. Constr. Build. Mater. 22, 2078–2086. https://doi.org/10.1016/j.conbuildmat.2007.07.019.

Y. Millogo, Etude géotechnique, chimique et minéralogique de matières premières argileuse et latéritique du Burkina Faso améliorées aux liants hydriques: application au génie civil (batiment et route), Thèse l'UNIVERSITE OUAGADOUGOU Burkina Faso. (2008) 157.

A. Mulyadi, Effect of water curing duration on strength behaviour of portland composite cement (PCC) mortar Effect of water curing duration on strength behaviour of portland composite cement (PCC) mortar, (2017). https://doi.org/10.1088/1757-899X/271/1/012018.

Obonyo, E.A., Kamseu, E., Lemougna, P.N., Tchamba, A.B., Melo, U.C., Leonelli, C., 2014. A sustainable approach for the geopolymerization of natural iron-rich aluminosilicate materials. Sustain 6, 5535–5553. https://doi.org/10.3390/su6095535.

O. Omotoso, O.J. Ojo, Engineering Properties of Lateritic Soils around Dall Quarry in Sango Area , Engineering Properties of Lateritic Soils around Dall Quarry in Sango Area , Ilorin , Nigeria, (2012). https://doi.org/10.5539/esr.v1n2p71.

Pourkhorshidi, A.R., Najimi, M., Parhizkar, T., Jafarpour, F., Hillemeier, B., 2010. Applicability of the standard specifications of ASTM C618 for evaluation of natural pozzolans. Cem. Concr. Compos. 32, 794–800. https://doi.org/10.1016/j.cemconcomp.2010.08.007.

D. Shi, P.W. Brown, lognormal Simulation of Pore Size Distributions in Cementitious Materials, 67 (1991) 1861–1867.

Tajuelo Rodriguez, E., 2015. Relation between composition, structure and morphology in C-S-H. Sch. Eng.. https://doi.org/10.1007/978-3-319-07109-1_9.

Tironi, A., Trezza, M.A., Scian, A.N., Irassar, E.F., 2013. Assessment of pozzolanic activity of different calcined clays. Cem. Concr. Compos. 37, 319–327. https://doi.org/10.1016/j.cemconcomp.2013.01.002.

Tironi, A., Castellano, C.C., Bonavetti, V., Trezza, M.A., Scian, A.N., Irassar, E.F., 2015. Blended cements elaborated with kaolinitic calcined clays. Procedia Mater. Sci. 8, 211–217. https://doi.org/10.1016/j.mspro.2015.04.066.

B.S. Waziri, Z.A. Lawan, M. Mala, B. Shehu Waziri, Z. Alhaji Lawan, aji Mala, Properties of Compressed Stabilized Earth Blocks (CSEB) for low- cost housing construction: a preliminary investigation, Int. J. Sustain. Constr. Eng. Technol. 4 (2013) 2180–3242. http://penerbit.uthm.edu.my/ojs/index.php/IJSCET.

Yanguatin, H., Tobón, J., Ramírez, J., 2017. Pozzolanic reactivity of kaolin clays, a review | Reactividad puzolánica de arcillas caoliníticas, una revisión. Rev. Ing. Constr. 32, 13–24.

Yu, P., Kirkpatrick, R.J., Poe, B., McMillan, P.F., Cong, X., 2004. Structure of calcium silicate hydrate (C-S-H): near-, mid-, and far-infrared spectroscopy. J. Am. Ceram. Soc. 82, 742–748. https://doi.org/10.1111/j.1151-2916.1999.tb01826.x.

Zhang, P., Duan, N., Dan, Z., Shi, F., Wang, H., 2018. An understandable and practicable cleaner production assessment model. J. Clean. Prod. 187, 1094–1102. https://doi.org/10.1016/j.jclepro.2018.03.284.

H. Zhao, Q. Xiao, D. Huang, S. Zhang, Influence of Pore Structure on Compressive Strength of Cement Mortar, 2014 (2014).

Zhou, J., Ye, G., van Breugel, K., 2010. Characterization of pore structure in cement-based materials using pressurization-depressurization cycling mercury intrusion porosimetry (PDC-MIP). Cem. Concr. Res. 40, 1120–1128. https://doi.org/10.1016/j.cemconres.2010.02.011.